Systematic in vitro biocompatibility studies of multimodal cellulose nanocrystal and lignin nanoparticles

Imlimthan, Surachet

2020-03

Imlimthan , S , Correia , A , Figueiredo , P I , Lintinen , K , Balasubramanian , V , Airaksinen , A , Kostiainen , M A , Almeida Santos , H & Sarparanta , M P 2020 , ' Systematic in vitro biocompatibility studies of multimodal cellulose nanocrystal and lignin nanoparticles ' , Journal of Biomedical Materials Research. Part A , vol. 108 , no. 3 , pp. 770-783 . https://doi.org/10.1002/jbm.a.3685

http://hdl.handle.net/10138/328535
https://doi.org/10.1002/jbm.a.36856

acceptedVersion

Systematic *In Vitro* Biocompatibility Studies of Multimodal Cellulose Nanocrystal and Lignin Nanoparticles

Surachet Imlimthan,[1] Alexandra Correia,[2] Patrícia Figueiredo,[2] Kalle Lintinen,[4] Vimalkumar Balasubramanian,[2] Anu J. Airaksinen,[1] Mauri A. Kostiainen,[4] Hélder A. Santos,[2,3] Mirkka Sarparanta[1,]*

[1]Department of Chemistry, Radiochemistry, University of Helsinki, Finland

[2]Drug Research Program, Division of Pharmaceutical Chemistry and Technology, Faculty of Pharmacy, University of Helsinki, Finland

[3]Helsinki Institute of Life Science, Helsinki, Finland

[4]Biohybrid Materials, Department of Bioproducts and Biosystems, Aalto University, Espoo, Finland

*Corresponding author: Mirkka Sarparanta, Department of Chemistry, Radiochemistry, P.O.Box 55, FI-00014 University of Helsinki, Finland, e-mail: mirkka.sarparanta@helsinki.fi.

Short title: *Cell viability assay compatibility with multimodal cellulose and lignin nanoparticles*

This article has been accepted for publication and undergone full peer review but has not been through the copyediting, typesetting, pagination and proofreading process which may lead to differences between this version and the Version of Record. Please cite this article as doi: 10.1002/jbm.a.36856

ABSTRACT

Natural biopolymer nanoparticles (NPs), including nanocrystalline cellulose (CNC) and lignin, have shown potential as scaffolds for targeted drug delivery systems due to their wide availability, cost-efficient preparation, and anticipated biocompatibility. Since both CNC and lignin can potentially cause complications in cell viability assays due to their ability to scatter the emitted light and absorb the assay reagents, we investigated the response of bioluminescent (CellTiter-Glo®), colorimetric (MTT® and AlamarBlue®) and fluorometric (LIVE/DEAD®) assays for the determination of the biocompatibility of the multimodal CNC and lignin constructs in murine RAW 264.7 macrophages and 4T1 breast adenocarcinoma cell lines. Here, we have developed multimodal CNC and lignin NPs harboring the radiometal chelator DOTA (1,4,7,10-tetraazacyclododecane-1,4,7,10-tetraacetic acid) and the fluorescent dye Cyanine 5 for the investigation of nanomaterial biodistribution *in vivo* with nuclear and optical imaging, which were then used as the model CNC and lignin nanosystems in the cell viability assay comparison. CellTiter-Glo® based on the detection of ATP-dependent luminescence in viable cells revealed to be the best assay for both nanoconstructs for its robust linear response to increasing NP concentration and lack of interference from either of the NP types. Both multimodal CNC and lignin NPs displayed low cytotoxicity and favorable interactions with the cell lines, suggesting that they are good candidates for nanosystem development for targeted drug delivery in breast cancer and for theranostic applications. Our results provide useful guidance for cell viability assay compatibility for CNC and lignin NPs and facilitate the future translation of the materials for *in vivo* applications.

KEYWORDS

cellulose nanocrystal, lignin nanoparticle, multimodal imaging probe, biocompatibility, cell viability

INTRODUCTION

Nanomaterials are intensely investigated as carriers for therapeutic payloads and diagnostic labels.[1,2] A number of nanocarrier-based drug delivery systems, for example, liposomes, micelles, protein conjugates, and polymers, are commercially available or in clinical trials.[3-5] Cellulose and lignin are important renewably-resourced natural biopolymers that have emerged as potential sources of nanoscale scaffolds in cosmetic, food packaging, and drug delivery applications. Nanocrystalline cellulose (CNC) has already been widely proposed suitable for biomedical applications.[6-10] CNC can be extracted from native cellulose obtained from various natural sources, for example bacteria,[11] animals,[12] and plants[13] where the crystalline regions of the cellulose are enriched over the amorphous regions through acid hydrolysis.[14] CNC typically has dimensions of 10–15 nm in diameter and 150–200 nm in length, showing a high aspect ratio and appearing as needle-like NPs under microscopic observation.[15] Lignin is the second most abundant component after cellulose in wood. Lignin is comprised of three aromatic alcohol structures, the *p*-coumaryl, coniferyl, and sinapyl alcohols. Lignin can form well-defined spherical nanoparticles with a size range of 200–500 nm.[16] Lignin-based materials are increasingly investigated in the field of renewable energy production as an alternative to fossil fuels.[17-20] Like CNC, lignin can be utilized in multifunctional materials for various biomedical applications, but the biomedical use of lignin is still in its infancy, and the reports on the biomedical use of CNC by far outnumber those on lignin.[21-25]

One of the most important characteristics of both CNC and lignin is the reactive surface covered with numerous reactive hydroxyl and other functional groups available for different types of chemical modification. This allows for the incorporation of a wide range of labels, therapeutic compounds and targeting vectors on their surface.[22,26] Due to the highly negative surface charge of

both materials, they form a well-dispersed colloidal suspension in aqueous media, which can prolong the circulation of CNC and lignin NPs in bloodstream as well as reduce the non-specific interaction with plasma proteins *in vivo*.[27-29] The cytotoxicity, biocompatibility and fate *in vivo* are major concerns in the development of nanomaterials for biomedical applications.[30] In a few preceding reports, nanoscale cellulose and lignin have been shown to be relatively non-toxic and well tolerated in cell models.[26,31-33] However, as any chemical modification is likely to affect the physicochemical properties of the material important for the biocompatibility and cellular interactions, such as surface chemistry, morphology, degree of crystallinity and dispersion stability, the biocompatibility of any new nanomaterial construct should be rigorously evaluated before *in vivo* use.[34,35]

In this study, we investigated the cytotoxicity of two multimodal CNC and lignin constructs systematically using a number of commercially available cell viability assays. Both CNC and lignin NPs have the potential to interfere with the readout in the assays due to adsorption of the assay reagents and dampening or scattering of the optical signal, resulting in erroneous results. The cell viability assays used in this study were based on luminescent (CellTiter-Glo®), colorimetric (MTT® and AlamarBlue®) and fluorometric (LIVE/DEAD®) detection. The radiometal chelator DOTA (1,4,7,10-tetraazacyclododecane-1,4,7,10-tetraacetic acid) and fluorescent dye Cy5 -modified CNC[36] and lignin NPs (this study) were developed to generate multimodality imaging probes for single-photon emission computed tomography (SPECT) and optical imaging (**Scheme 1**), and are used here as model modified CNC and lignin constructs for the systematic comparison of the cell viability assays. The cytotoxicity and cell interactions of the prepared CNC and lignin constructs were evaluated in murine RAW 264.7 macrophages and in murine 4T1 breast adenocarcinoma cell lines as the first step of their evaluation for *in vitro* and *in vivo* applications.

EXPERIMENTAL SECTION

Materials and chemicals

Cellulose nanocrystal (CNC) was generated from acid hydrolysis of cotton fibres (Whatman® filter paper) as described in the literature.[37,38] The acid and sulphate residues of CNC were washed out with 5 changes of DMSO and 2 changes of ultrapure water (10 ml each wash) before collecting the CNC pellet back by lyophilization. Softwood kraft lignin in aqueous solution was prepared as described in the literature.[16] All chemicals, organic solvents, and cell viability assays were purchased from Sigma-Aldrich (St. Louis, MO, USA), VWR (Radnor, PA, USA), Lumiprobe GmbH (Hannover, Germany), Macrocyclics (Plano, TX, USA), Thermo Fisher Scientific (Waltham, MA, USA), and Promega (Madison, WI, USA), and were used without additional purification. The dialysis tubing and membrane were obtained from Spectrum Labs (Rancho Dominguez, CA, USA). The ultrapure water (18.2 MΩ) was prepared by a Milli-Q Integral 10 water purification system. The cell culture conditions, cell viability assays and other procedures for cell experiments are described in the Supporting Information (SI).

Multimodal cellulose nanocrystal and lignin preparation

Multimodal cellulose nanocrystals were prepared by the conjugation of DOTA-NH-NH_2 (1,4,7,10-tetraazacyclododecane-1,4,7-tris (acetic acid)-10-acethydrazide), which was synthesized in-house from amide coupling reaction of 1,4,7,10-tetraazacyclododecane-1,4,7-tris-tert-butyl acetate-10-acetic acid precursor (DOTA-tris(*t*-Bu ester) (Macrocyclics) or fluorescent dye Cy5-NH-NH_2 (Lumiprobe) to the terminal aldehyde of CNC through hydrazide-aldehyde coupling reaction.[36] The cellulose nanocrystals were dispersed in anhydrous DMSO at the concentration of 5 mg/ml. The CNC solution was sonicated with tip sonicator (tip diameter 3 mm, SONIC® Inc., Newtown, CT, USA) at 20% amplitude for 5 min, and then the solution was flushed with argon flow for 10 min while stirring. The DOTA-NH-NH_2 (1 eq w/w) or Cy5-NH-NH_2 (0.3 eq w/w) was added to the CNC dispersion under argon atmosphere. The reaction was left stirring under argon at 50–60 °C for 4 days. The reaction mixture was transferred to a conical centrifuge tube and centrifuged at 4000

rpm, 5 min to collect the DOTA- or Cy5-CNC product. The DOTA-CNC pellet was washed with 4 exchanges of fresh DMSO while Cy5-CNC was washed with DMSO until the supernatant became colorless. The multimodal CNC products were further purified against ultrapure water in a dialysis tube (MWCO 3.5–5.0 kDa) for 4 days. The ultrapure water was changed at least twice a day. The obtained DOTA- or Cy5-CNC in aqueous solution was dried and collected in powder form by lyophilization.

Multimodal lignin NPs were prepared by the activation of hydroxyl groups through 1,1'-carbonyldiimidazole (CDI)-mediated amine coupling reaction. Lignin was dissolved in anhydrous THF at the concentration of 5 mg/ml. CDI (3 eq w/w) was separately dissolved in anhydrous THF, and then slowly added to the lignin solution under argon flow. The activation reaction was run under argon atmosphere at 40–50 °C overnight. Then, 0.3 eq (w/w) of DOTA-NH_2 (1,4,7,10-tetraazacyclododecane-1,4,7-tris (acetic acid)-10-(4-aminobutyl) acetamide (Macrocylics) or 0.03 eq of Cy5-NH_2 (Lumiprobe) was added to the CDI-activated lignin reaction mixture. The reaction was further left stirring under argon atmosphere at 40–50 °C for 3 days. The multimodal lignin products were solvent exchange in dialysis membrane (MWCO 12–14 kDa) immersed in ultrapure water for 3 days while ultrapure water was changed at least twice a day. The final products were collected by lyophilization.

Material characterization

The elemental compositions of CNC and lignin were analyzed by a Vario MICRO Cube CHNS analyzer (Elementar Analysensysteme GmbH, Langenselbold, Germany) reported as percent compositions (C, H, and N). The Fourier Transform Infrared Spectroscopy (FTIR, Vertex 70, Bruker, MA, USA) equipped with Attenuated Total Reflectance (ATR, MIRacle, PIKE Technologies, WI, USA) was used to confirm the covalent conjugation of DOTA and Cy5 to the CNC and lignin. The hydrodynamic diameter and surface charge (ζ–potential) of unmodified and modified CNC/lignin were characterized with Malvern Zetasizer Nano ZS instrument (Malvern,

Worcestershire, UK). The dimensions and morphology of unmodified and modified CNC/lignin constructs were observed by transmission electron microscopy (TEM) at 120 kV (Tecnai 12 Bio-Twin FEI, Hillsboro, OR, USA). The unmodified and modified CNC/lignin were dispersed in ultrapure water and sonicated for 5 min. The 5 µl of each CNC/lignin suspension were applied on a glow discharge treated carbon support film hexagonal 300 mesh copper grids (Electron Microscopy Sciences, PA, USA). The CNC samples were further stained with 1% uranyl acetate for 2 min while lignin samples were left without staining. The samples were gently blotted out from the edge of the grid with filter paper before air-drying at least 2 h prior to the measurements.

In vitro stability studies of multimodal CNC and lignin nanoparticles

The *in vitro* stability of multimodal CNC and lignin NPs was carried out in 1×PBS (pH 7.4), 50% human plasma, and complete cell culture medium, DMEM supplemented with 10% FBS, 1% non-essential amino acids (NEAA), 1% L-glutamine and 1% penicillin-streptomycin. The concentration was 300 µg/ml and the samples were incubated at 37 °C with constant shaking at 300 rpm. The samples were drawn at 6, 24, and 48 h for size and ζ-potential measurements. All experiments were performed in triplicate. Due to the strong light scattering of CNC in the Zetasizer measurement, the stability of the CNC NPs in terms of size and morphology was studied by TEM.

Cell viability studies

The *in vitro* cell viability studies were carried out using luminescent CellTiter-Glo® (Promega Corp., Madison, WI, USA) and fluorescent LIVE/DEAD® (Thermo Fisher Scientific, Waltham, MA, USA) assays in murine RAW 264.7 macrophages and murine 4T1 adenocarcinoma cell lines at 6, 24, and 72 h. In addition, we tested two widely used cell viability assays, the colorimetric MTT® (Sigma-Aldrich, St. Louis, MO, USA) and AlamarBlue® (Thermo Fisher Scientific Waltham, MA, USA), for comparison in the RAW 264.7 macrophages at 6 and 24 h. The procedures for both additional assays are detailed in the SI.

CellTiter-Glo® assay

Murine RAW 264.7 macrophages and murine 4T1 breast adenocarcinoma cell lines were seeded in 96-well plate (Corning® 3610, NY, USA) at a density of 15 000 cells per well in 100 µl DMEM and RPMI-1640, respectively. The cells were allowed to attach overnight. The media were discarded and replaced with 100 µl of unmodified-CNC/lignin, DOTA-CNC/lignin, and Cy5-CNC/lignin NPs in corresponding media at 5, 25, 100, 250, 500, and 1000 µg/ml. The fresh media and 1% (v/v) Triton X-100 were added and used as negative and positive controls, respectively. The cells were incubated at 37 °C, 5% CO_2, and 95% relative humidity for 6, 24, and 72 h. At predetermined time point, the plates were equilibrated to room temperature for 30 min. The cells were washed twice with Hank's balanced salt solution (HBSS) supplemented with 10 mM HEPES (HBSS-HEPES, pH 7.4). Then, 50 µl of each HBSS-HEPES and CellTiter-Glo® assay reagent was added to the wells. The plates were gently shaken for 2 min and incubated at room temperature for 30 min in the dark. The luminescence was measured with Varioskan LUX multimode microplate reader (Thermo Fisher Scientific, Waltham, MA, USA). All measurements were carried out in triplicate.

LIVE/DEAD® assay

Both cell lines were plated at 25 000 cells per well in 1.5 Nunc Lab-Tek® II 8-chambered cover glasses (Thermo Fisher Scientific, Waltham, MA, USA). The media was discarded and replaced with 200 µl of unmodified-CNC/lignin, DOTA-CNC/lignin, and Cy5-CNC/lignin NPs dispersed in the corresponding media at concentrations of 5, 25, 100, 250, 500, and 1000 µg/ml. The cells were incubated for 6, 24, and 72 h under the same conditions as for the CellTiter-Glo® assay. At the designated time points, the cells were washed twice with phosphate buffered saline (1×PBS, pH 7.4). One of the control wells was treated with 200 µl of 0.1% (w/w) saponin for 10 min at room temperature as a positive control while the other wells were supplemented with 1×PBS (pH 7.4). After 10 min incubation, the saponin solution was carefully removed and the cells were washed once with 1×PBS (pH 7.4). Then, the PBS in all wells was discarded and 150 µl of Calcein

AM/EthD-1 staining solution were added to each well. The preparation of staining solution is described in the SI. The cells were incubated with the staining solution at room temperature for 45 min in the dark. Cell images were taken by confocal fluorescence microscope (Leica TCS SP5II, Leica Microsystems, Wetzlar, Germany) at 20× magnification. The images were captured in different areas of the well. The number of live and dead cells (n > 100 cells) were counted using the Fiji ImageJ 1.51 software.

In vitro cell–nanoparticle interactions

The interactions between both cell lines (RAW 264.7 and 4T1) and Cy5-CNC/lignin NPs were qualitatively studied with confocal fluorescence microscopy at 63× magnification. The cells were seeded at a density of 50,000 cells per well in 1.5 Nunc Lab-Tek® II 8-chambered cover glasses and allowed to attach overnight. The media was removed and replaced with Cy5-CNC/lignin NPs solutions at a concentration of 100 µg/ml prepared in complete cell culture medium. The cells were incubated with the samples at 37 °C, 5% CO_2, and 95% relative humidity for 6 and 24 h. At the time point, the cells were washed once with 1×PBS (pH 7.4) and 200 µl of CellMask™ Green solution (Thermo Fisher Scientific Inc., Waltham, MA, USA) (5µg/ml in 1×PBS) were added to stain the cell membrane for 3 min in the 37 °C incubator. The cell membrane staining solution was discarded and the cells were washed once with 1×PBS before fixation with 200 µl of 4% paraformaldehyde (PFA) at 37 °C for 15 min. After fixing, the cells were washed twice with 1×PBS and the nuclei were subsequently stained with 200 µl of DAPI solution (2.48 µg/ml in 1×PBS) for 5 min in the 37 °C incubator. Then, the cells were washed once with 1×PBS and 200 µl of fresh 1×PBS was added to each well. The cell-NPs interactions were observed under confocal fluorescence microscope by detecting the fluorescent signals from Cy5 (649/666 nm) on CNC/lignin NPs, DAPI (350/470 nm), and CellMask™ Green (522/535 nm). The images were analyzed with Fiji ImageJ 1.51 software.

RESULTS

Multimodal cellulose and lignin characterization

In this study, the multimodal cellulose nanocrystals, DOTA-CNC and Cy5-CNC, were prepared through hydrazide-aldehyde coupling reaction by conjugating DOTA- and Cy5-hydrazide to the aldehyde group at the reducing end of CNC.[36] The multimodal lignin, DOTA-lignin and Cy5-lignin, were prepared by random CDI-activation of the hydroxyl groups on the surface of lignin and followed by conjugation of either DOTA-amine and Cy5-amine. The successful conjugation of DOTA and Cy5 on both CNC and lignin were confirmed with ATR-FTIR spectroscopy. According to the FTIR spectrum of CNC, the indicated amide II peak (C-H stretching and N-H bending) appeared at 1590 cm^{-1}, while the corresponding amide I peak (C=O stretching) was detected at 1665 cm^{-1} (**Figure S1A**). For the FTIR spectrum of lignin, the amide III (C-N stretching) appeared at 1384 cm^{-1}, while the carbonyl vibration (C=O stretching) from carboxylic group was seen at 1760 cm^{-1} (**Figure S1B**), confirming the successful conjugation of DOTA and Cy5 to CNC and lignin.

Furthermore, the elemental analysis was carried out to quantify the elemental composition of unmodified and modified CNC and lignin materials (**Table 1**). The nitrogen (N) content was increased to 0.1% in DOTA-CNC and Cy5-CNC, while the N content in unmodified CNC is undetectable. In the modified lignin materials, the nitrogen content was also increased from undetectable to 5.5 and 1.5% for DOTA-lignin and Cy5-lignin, respectively. However, there are no differences in carbon (C) and hydrogen (H) contents observed. The dispersion characteristics, including size and polydispersity index (PDI) of CNC and lignin NPs in aqueous solution, were measured by dynamic light scattering (DLS), as indicated in **Figure 1 and Table S1**. The unmodified lignin NPs show a hydrodynamic diameter less than 200 nm with a narrow size distribution (PDI=0.138), which is suitable for use as a drug carrier. However, the conjugation of DOTA and Cy5 on the surface of lignin NPs increased the hydrodynamic radii and polydispersity to

606 nm (PDI=0.637) and 545 nm (PDI=0.354) for DOTA-lignin and Cy5 lignin, respectively. The dimensions of CNC, including width and length, were characterized by TEM. In TEM, the CNC NPs showed a needle-like shape with average width of 15 nm and length of 170 nm both before and after DOTA and Cy5 conjugations (**Figure 2A and Figure S2**). On the other hand, the unmodified and modified lignin NPs maintained a spherical shape but the size of modified NPs was increased and a less uniform distribution compared to the unmodified NPs was seen (**Figure 2B**). The observations are in agreement with the DLS results. Furthermore, there was a slight decrease of the surface charge due to the decrease in number of hydroxyl groups in both nanomaterials after the modifications (**Figure 1**).

In vitro stability of nanoparticles

Since it is also important to study the interaction between plasma proteins and NPs to monitor the potential change of the NP characteristics governing *in vivo* biodistribution – the surface charge, size, and shape – the *in vitro* stability of CNC and lignin NPs was investigated under simulated physiological conditions. The NPs were incubated at 37 ˚C for 6, 24, and 48 h in 1×PBS (pH 7.4) and in 50% human plasma. The changes in size and ζ-potential of the CNC and lignin NPs was measured by DLS, however, the size observation of CNC NPs was done by TEM because of its strong light scattering property in the DLS. By TEM, the CNC NPs showed a good stability in both 1×PBS and 50% human plasma, with the nanocrystal dimensions and ζ-potential remaining constant over the 48-hour incubation period (**Figure 3**). The unmodified lignin NPs maintained constant size, PDI and ζ-potential in 1×PBS over the incubation period, however, the size was increased from 150 to 300 nm after 6 h incubation in 50% human plasma, indicative of protein adsorption on the surface of NPs. The DOTA- and Cy5-modified lignin NPs were stable under both simulated physiological conditions, maintaining constant size and ζ-potential over the incubation period (**Figure 4**).

In vitro cell viability

The *in vitro* cell viability assays were carried out at concentrations of CNC and lignin NPs ranging from 5–1000 µg/ml with 6, 24, and 72 h incubation in murine RAW 264.7 macrophages and murine 4T1 mammary adenocarcinoma cell lines. To simplify the discussion, we will from here on denote the concentrations as either low (5, 25 and 100 µg/ml) or high (250, 500 and 1000 µg/ml) ranges, as there is a clear step in the cell viability when the concentration increases from 100 to 250 µg/ml. All CNC and lignin NPs showed very good biocompatibility with RAW 264.7 macrophages at the low concentration range at 6 and 24 h, with cell viability higher than 90% in both CellTiter-Glo® (**Figure 5A** and **B**) and LIVE/DEAD® (**Figure 6A** and **B**) assays. However, the number of viable cells was less than 80% after 72 h incubation, the time dependent manner triggering cell death induced by the CNC and lignin NPs in the low concentration range (**Figure 5C** and **6C**). At the high concentration range, all NPs showed cytotoxicity already after 6 h incubation in the CellTiter-Glo® assay (**Figure 5A–C**), with cell viability of less than 50% and a linear decreasing trend over the concentration range. However, the cell viability results from LIVE/DEAD® assay at the high concentration range fluctuated over the incubation period (**Figure 6A** and **B**). Furthermore, the half-maximal inhibitory concentration (IC_{50}) of CNC and lignin NPs was determined from the CellTiter-Glo® assay. The average IC_{50} values of CNC and lignin NPs for RAW 264.7 macrophages were 878 and 847 µg/ml at 6 h, 241 and 202 µg/ml at 24 h, and 99 and 91 µg/ml at 72 h incubation, respectively.

In 4T1 cells, all NPs yielded a cell viability higher than 80% over the incubation period at the low concentration range in both CellTiter-Glo® (**Figure 5D–F**) and LIVE/DEAD® (**Figure 6D–F**) assays. The CellTiter-Glo® assay only was selected to further investigate the cytotoxicity at the high concentration range in 4T1 cell line since we already had an indication of the unsuitability of the LIVE/DEAD® assay from the RAW 264.7 experiment because of the loss of dead cells in the assay preparation as further discussed. The cell viability was over 80% after 6 h incubation, but the NPs

started to become toxic to the cells in the subsequent time points, and the viability dropped to below 70% (**Figure 5A-C**). The average IC_{50} values of CNC and lignin NPs for 4T1 cell line were 2570 and 2531 µg/ml at 6 h, 1440 and 1294 µg/ml at 24 h, and 1064 and 490 µg/ml at 72 h incubation, respectively.

In addition, the colorimetric MTT® and AlamarBlue® assays were carried out in RAW 264.7 macrophages in order to investigate the compatibility of these widely-employed cytotoxicity assays with CNC and lignin NPs, and to compare to the results obtained from the CellTiter-Glo® and LIVE/DEAD® assays. Overall, both MTT® and AlamarBlue® assays revealed an increasing trend in cell viability when the NPs concentration and incubation time were increased (**Figure S4**) indicative of the adsorption and reduction of the assay reagents on the nanomaterials. Consequently, the IC_{50} values were not determined for the MTT® and AlamarBlue® assays.

In vitro cell–nanoparticle interactions

In this experiment, we evaluated qualitatively the cell interaction (cellular association and/or internalization) of Cy5-labelled CNC and lignin NPs with confocal fluorescence microscopy after incubation for 6 and 24 h at a concentration of 100 µg/ml, the non-cytotoxic limit determined in the earlier assays. RAW 264.7 macrophages and 4T1 mammary adenocarcinoma cells were used to model NP interactions in immune and cancer cells, respectively. Cy5-CNC NPs demonstrated a strong interaction in both immune and cancer cell lines over the incubation period (**Figure 7A–D**). Cy5-lignin NPs revealed a good interaction only with RAW 264.7 macrophages at 24 h (**Figure 7C**) but not with the 4T1 cell line (**Figure 7B and D**).

DISCUSSION

In the present work, we have developed the multimodal CNC (DOTA-CNC and Cy5-CNC) and lignin (DOTA-lignin and Cy5-lignin) NPs to facilitate the *in vitro* and *in vivo* evaluation of these nanoconstructs for drug delivery applications. ATR-FTIR analysis confirmed the successful

conjugation of DOTA and Cy5 to CNC and lignin materials. According to the elemental analysis, there are no significant differences in the carbon (C) and hydrogen (H) content between unmodified and modified CNC/lignin due to the fact that C and H are major components in both biomaterials. Therefore, chemical modifications do not have a substantial effect on changing the proportions of those elements in the high molecular weight biopolymer. However, the nitrogen content in DOTA and Cy5-modified lignin materials was higher than in DOTA and Cy5-modified CNC because the hydroxyl groups on lignin were randomly activated, resulting in arbitrary conjugation of DOTA/Cy5-amine while each CNC has approximately one aldehyde group available for the conjugation of DOTA/Cy5-hydrazide. The increase in the nitrogen content in both modified materials is indicative of successful functionalization with DOTA and Cy5. Furthermore, the dispersion characteristics of CNC and lignin NPs was determined by DLS. In DLS, the size of modified lignin NPs was increased to approximately 3 times from the unmodified lignin NPs. Although the size of NPs for drug delivery systems is preferentially smaller than 200 nm,[39] the NPs used for the passive targeting of tumor vasculature via the enhanced permeability and retention (EPR) effect can be in the range of 200–780 nm.[40] However, further optimization of the conjugation chemistry of DOTA and Cy5 to the lignin NPs to maintain the optimal size of the lignin NPs (<200 nm) is warranted.

Because CNC are non-spherical NPs, the width and length determinations by DLS become more complex, where the light scattering needs to be measured in multiple angles to obtain accurate dimensions while the spherical NPs give the same scattering pattern from all direction of the particle. Moreover, CNC is not optically transparent in aqueous solution, resulting in strong light scattering during the measurement and causing erroneous results.[41,42] Therefore, the most appropriate method for morphological characterization of CNC NPs is transmission electron microscopy (TEM).

The surface charge of NPs is one of the most important factors for the evaluation of dispersion stability, material-cell surface interaction, and for the nonspecific adsorption of plasma proteins.[43,44] The surface charge of both nanomaterials was slightly decreased after the chemical modifications. However, the NPs still maintained a negatively charged surface, which can promote a dispersion stability through electrostatic repulsion. Furthermore, negative surface charge lessens the chance of non-specific plasma protein adsorption that might result in rapid clearance of NPs from the blood circulation *in vivo* by the mononuclear phagocyte system (MPS).[45,46]

As CNC and lignin NPs behave as colloidal materials in aqueous solution, the stability of those NPs in simulated physicochemical conditions needs to be explored because NPs can become unstable through nonspecific adsorption of proteins and the loss in surface charge properties resulting in aggregation. Both the unmodified and Cy5- and DOTA-modified CNCs revealed constant dimensions and ζ-potential in 1×PBS and 50% human plasma, indicating good dispersion stability of the material in physiological fluids. On the other hand, the size, PDI and ζ-potential of lignin NPs were all altered by incubation in the simulated conditions. The unmodified lignin NPs were stable only in 1×PBS while the size was doubly increased in 50% human plasma, which indicates the possibility of nonspecific protein adsorption on the surface of lignin NPs. However, the size and ζ-potential of the Cy5- and DOTA-modified lignin NPs were preserved in the simulated conditions. In addition, the *in vitro* stability of all NPs was also tested in the cell culture medium used in the *in vitro* studies. The results were similar as for PBS and 50% human plasma, with the size and ζ-potential remaining constant over the 48-hour incubation period for all of the materials studied (**Figure S3**).

The chemical functionalization of the surface can alter the NP behavior in biological systems due to the effects on surface chemistry, morphology, charge density and size, resulting in decrease in the biocompatibility of the material. Herein, we evaluated the cell viability after incubation with CNC and lignin NPs using different commercially available cell viability assays to determine the possible

material interference in these assays and to select an appropriate one for future *in vitro* evaluations of CNC and lignin-based drug delivery systems. We studied the biocompatibility of NPs in murine RAW 264.7 macrophage cell line as an innate immune cell model that NPs would be cleared by tissue-resident and circulating macrophages after systemic administration *in vivo*. Furthermore, we also carried out the cytotoxicity study in murine 4T1 mammary adenocarcinoma cell line in order to investigate the potential of CNC and lignin NPs for drug delivery applications in oncology. According to the results, both CNC and lignin NPs revealed good biocompatibility with RAW 264.7 macrophage and 4T1 cell lines in both CellTiter-Glo® and LIVE/DEAD® assays in the low concentration range while the cytotoxicity was increased in the high concentration range. However, the result fluctuated significantly in the LIVE/DEAD® assay over the incubation period. This is probably representative of the loss of dead cells during the washing step in the confocal microscopy sample preparation. Therefore, the number of the dead cells is not accurately quantified, which affects the percent cell viability calculation. This effect may not be clearly seen in the low concentration range because the number of viable cells in general is higher (> 90%). In contrast, the percent cell viability in the CellTiter-Glo® assay is determined based on the luminescent signal, which is proportional to the amount of ATP produced by living cells regardless of the presence or absence of dead cells, which simplifies the sample preparation and makes the cell viability determination more accurate. No interference of the nanomaterials with the CellTiter-Glo® assay reagent was observed with either CNC or lignin NPs. Neither CNC nor lignin NPs showed any significant cytotoxicity up to 100 µg/ml in both cell models. When comparing the average IC_{50} values of CNC and lignin NPs in the RAW 264.7 and 4T1 cell lines, the average IC_{50} values in the 4T1 cell line are higher than in the RAW 264.7 macrophages. This might be an effect from the potential of cancer cells to evade from the self-destruction signals unlike normal cells, allowing them to survive when exposed to cytotoxic nanomaterials.[47,48] This behavior can cause resistance to drugs and nanoparticles in cancer therapy. Although the precise resistance mechanisms to

nanomaterial toxicity in cancer are still unclear, the mechanisms could include the activation of anti-apoptosis, enhanced cell proliferation and pro-survival pathways.[49,50] Moreover, the high IC_{50} values of CNC and lignin NPs in both RAW 264.7 and 4T1 indicate low potential to cause acute toxicity and can help to determine a safe starting dose level for *in vivo* investigations. However, the toxic concentration of nanomaterials in *in vitro* assays provides the corresponding information to the dose-response in 2D cell culture only, in conditions strikingly different from tissues *in vivo*. Therefore, the actual dose of nanomaterials delivered *in vivo* without adverse effects has to be evaluated carefully.[51] Constructs bearing imaging labels such as fluorochromes and radiometal chelators like those utilized in this work are valuable tools to this end as they allow for the visualization of nanomaterial behavior and quantification of the NP biodistribution *in vivo* with non-invasive imaging.[36] Evaluation of the *in vitro* biocompatibility and cytotoxicity of labeled nanomaterials is all the more important as the labeling strategy chosen should not affect the nanomaterial behavior in biological systems compared to the non-labeled material.

In the colorimetric AlamarBlue® and MTT® assays also widely employed for investigations of nanomaterial cytotoxicity, both CNC and lignin nanomaterials showed an increased trend of viability with increasing NP concentration and incubation time, in stark contrast to the findings of the Cell-TiterGlo® assay. Although cell viability in these assays is determined through the redox reaction that undergoes a colorimetric change of the assay reagent in response to the metabolic reduction in living cells, there may have been residual CNC and lignin NPs left on the cell membrane that can absorb the assay reagents on their high specific surface area resulting in the increase of the observed signal in the measurement. This effect can be problematic, especially in the AlamarBlue® assay in which the NPs are not washed out before adding the assay reagent. Therefore, the assay protocols for both the MTT® and AlamarBlue® assays should be modified to ensure diligent removal of the NPs prior to adding the assay reagents, but this might also result in a disproportionate loss of the dead cells from the wells complicating the viability analysis. The MTT

assay has previously been determined unsuitable for cytotoxicity evaluation of mesoporous silica microparticles due to the reduction of the assay reagent by the particles themselves and it is possible that this phenomenon occurs also with CNC and lignin NPs.[52]

The ultimate goal of nanoscale drug delivery system development is to deliver the diagnostic and therapeutic payload with the carriers to the target effectively. There are many factors that can influence the interactions of the NPs with cells including surface charge and chemistry, NP shape, aspect ratio, size and dispersion stability of the NPs in biological systems.[53] The surface charge of NPs affects the avidity and strength of the cell membrane interactions with neutral charge considered to be optimal for avoiding unwanted NP-cell interactions.[44] Both Cy5-CNC/lignin NPs have a negatively charged surface, which can induce strong adhesion between the NPs and the cell membrane. Moreover, the particle morphology is considered to be an important parameter affecting the cellular interactions, circulation rheology, uptake kinetics, and internalization mechanisms.[54,55] In general, spherical NPs exhibit better cell interaction than non-spherical NPs due to a shorter membrane-wrapping time compare to sharp-end cylindrical NPs for which cells need additional energy to encapsulate and internalize.[35] However, the interaction and internalization mechanisms for non-spherical NPs are not fully understood and vary depending on particle orientation and the greatest dimension of the NP.[56,57] Therefore, we speculated that the lower interaction of Cy5-lignin NPs might be a result from the larger size of the NPs (>500 nm) for which cellular internalization might not be efficiently achieved within the observation period despite the optimal spherical shape.

CONCLUSION

In this paper, several *in vitro* cell viability assays were systematically evaluated for biocompatibility studies with cellulose nanocrystal and lignin-based nanoparticles intended for multimodal *in vivo* imaging of drug delivery system biodistribution. The multimodal CNC and lignin NPs maintained a highly negatively charged surface indicative of good dispersion stability. The unmodified and

modified CNC NPs were needle-shaped with the average dimensions of 15 nm in width and 170 nm in length, with a high aspect ratio and surface area, which could be beneficial for loading diagnostic and therapeutic agents for drug delivery applications. The unmodified lignin NPs showed a spherical shape with an average diameter of 170 nm while the conjugation of DOTA and Cy5 on lignin NPs increased their diameter to 500–600 nm. The conjugation chemistry for DOTA and Cy5 needs to be further optimized to reduce the increase in size and polydispersity of the modified lignin NPs. In addition, CNC and lignin NPs displayed a good *in vitro* stability in physiological media. The cell viability studies in murine RAW 264.7 macrophages and 4T1 breast adenocarcinoma cell lines revealed CellTiter-Glo® to be the most suitable cell viability assay for the *in vitro* evaluation of CNC and lignin NPs due to its linear response to the increasing of NP concentration and less interference from NP residues, which caused aberrant increase in the positive signal in colorimetric MTT® and AlamarBlue® assays. The fluorescent confocal-microscopic LIVE/DEAD® assay revealed to have a linear response to the increasing NP concentration, but the loss of dead cells at the high concentration range wells during the assay procedure resulted in cell viability values higher than true. Both multimodal CNC and lignin NPs demonstrated low cytotoxicity at concentrations below 100 µg/ml. Moreover, the multimodal CNC and lignin NPs revealed an interaction with high biocompatibility in both immune and cancer cell lines *in vitro*. Overall, the cytotoxicity and cellular interactions of CNC and lignin NPs suggest the possibility to use these materials as scaffolds for the future development of multimodal CNC and lignin-based drug delivery systems for oncologic applications, and the presented systematic evaluation of the different cytotoxicity assays will facilitate the *in vitro* evaluation of such constructs in the future.

SUPPORTING INFORMATION

Cell culturing materials and methods, MTT® and AlamarBlue® assays, ATR-FTIR characterization, CNC size distribution, CNC and lignin NPs stability test in complete cell culture medium, and results for cell viability in RAW 264.7 macrophages by MTT® and AlamarBlue® assays (PDF).

CONFLICT OF INTEREST

The authors declare no conflict of interests.

ACKNOWLEDGMENTS

Financial support from the Academy of Finland (Decision Nos. 278056, 308578, 303804, 273645, 264749, and 272579), Sigrid Juselius Foundation (Decision No. 4704580), Finnish Cultural Foundation (Decision No. 00170202), HiLIFE Research Funds, and University of Helsinki Research Funds are gratefully acknowledged. The authors also thank to Ms. Karina Moslova for the assistance in the elemental analysis.

REFERENCES

1. Bamrungsap S, Zhao Z, Chen T, Wang L, Li C, Fu T, Tan W. Nanotechnology in therapeutics: a focus on nanoparticles as a drug delivery system. Nanomedicine (Lond) 2012;7(8):1253-1271.
2. Liu D, Yang F, Xiong F, Gu N. The Smart Drug Delivery System and Its Clinical Potential. Theranostics 2016;6(9):1306-1323.
3. Lian T, Ho RJ. Trends and developments in liposome drug delivery systems. J Pharm Sci 2001;90(6):667-680.
4. Matsumura Y, Hamaguchi T, Ura T, Muro K, Yamada Y, Shimada Y, Shirao K, Okusaka T, Ueno H, Ikeda M and others. Phase I clinical trial and pharmacokinetic evaluation of NK911, a micelle-encapsulated doxorubicin. Br J Cancer 2004;91(10):1775-1781.
5. Tagami T, Ozeki T. Recent Trends in Clinical Trials Related to Carrier-Based Drugs. J Pharm Sci 2017;106(9):2219-2226.
6. Tang J, Sisler J, Grishkewich N, Tam KC. Functionalization of cellulose nanocrystals for advanced applications. J Colloid Interface Sci 2017;494:397-409.

7. Lam E, Male KB, Chong JH, Leung AC, Luong JH. Applications of functionalized and nanoparticle-modified nanocrystalline cellulose. Trends Biotechnol 2012;30(5):283-290.

8. Grishkewich N, Mohammed N, Tang J, Tam KC. Recent advances in the application of cellulose nanocrystals. Curr Opin Colloid Interface Sci 2017;29:32-45.

9. Akhlaghi SP, Berry RC, Tam KC. Surface modification of cellulose nanocrystal with chitosan oligosaccharide for drug delivery applications. Cellulose 2013;20(4):1747-1764.

10. Peng BL, Dhar N, Liu HL, Tam KC. Chemistry and applications of nanocrystalline cellulose and its derivatives: A nanotechnology perspective. Can J Chem Eng 2011;89(5):1191-1206.

11. George J, Ramana KV, Bawa AS, Siddaramaiah. Bacterial cellulose nanocrystals exhibiting high thermal stability and their polymer nanocomposites. Int J Biol Macromol 2011;48(1):50-57.

12. Azizi Samir MAS, Alloin F, Sanchez J-Y, Dufresne A. Cellulose nanocrystals reinforced poly(oxyethylene). Polymer 2004;45(12):4149-4157.

13. Ng H-M, Sin LT, Tee T-T, Bee S-T, Hui D, Low C-Y, Rahmat AR. Extraction of cellulose nanocrystals from plant sources for application as reinforcing agent in polymers. Compos Part B: Eng 2015;75:176-200.

14. Qua EH, Hornsby PR, Sharma HSS, Lyons G. Preparation and characterisation of cellulose nanofibres. J Mater Sci 2011;46(18):6029-6045.

15. Wang QQ, Zhu JY, Reiner RS, Verrill SP, Baxa U, McNeil SE. Approaching zero cellulose loss in cellulose nanocrystal (CNC) production: recovery and characterization of cellulosic solid residues (CSR) and CNC. Cellulose 2012;19(6):2033-2047.

16. Lievonen M, Valle-Delgado JJ, Mattinen M-L, Hult E-L, Lintinen K, Kostiainen MA, Paananen A, Szilvay GR, Setälä H, Österberg M. A simple process for lignin nanoparticle preparation. Green Chem 2016;18(5):1416-1422.

17. Parsell T, Yohe S, Degenstein J, Jarrell T, Klein I, Gencer E, Hewetson B, Hurt M, Kim JI, Choudhari H and others. A synergistic biorefinery based on catalytic conversion of lignin prior to cellulose starting from lignocellulosic biomass. Green Chem 2015;17(3):1492-1499.

18. Bu Q, Lei H, Wang L, Wei Y, Zhu L, Zhang X, Liu Y, Yadavalli G, Tang J. Bio-based phenols and fuel production from catalytic microwave pyrolysis of lignin by activated carbons. Bioresour Technol 2014;162:142-147.

19. Saidi M, Samimi F, Karimipourfard D, Nimmanwudipong T, Gates BC, Rahimpour MR. Upgrading of lignin-derived bio-oils by catalytic hydrodeoxygenation. Energy Environ Sci 2014;7(1):103-129.

20. Sathitsuksanoh N, Holtman KM, Yelle DJ, Morgan T, Stavila V, Pelton J, Blanch H, Simmons BA, George A. Lignin fate and characterization during ionic liquid biomass pretreatment for renewable chemicals and fuels production. Green Chem 2014;16(3):1236-1247.

21. Figueiredo P, Lintinen K, Hirvonen JT, Kostiainen MA, Santos HA. Properties and chemical modifications of lignin: Towards lignin-based nanomaterials for biomedical applications. Prog Mater Sci 2018;93:233-269.

22. Figueiredo P, Ferro C, Kemell M, Liu Z, Kiriazis A, Lintinen K, Florindo HF, Yli-Kauhaluoma J, Hirvonen J, Kostiainen MA and others. Functionalization of carboxylated lignin nanoparticles for targeted and pH-responsive delivery of anticancer drugs. Nanomedicine (Lond) 2017;12(21):2581-2596.

23. Laurichesse S, Avérous L. Chemical modification of lignins: Towards biobased polymers. Prog Polym Sci 2014;39(7):1266-1290.

24. Thakur VK, Thakur MK. Recent advances in green hydrogels from lignin: a review. Int J Biol Macromol 2015;72:834-847.

25. Zhou W, Zhang H, Chen F. Modified lignin: Preparation and use in reversible gel via Diels-Alder reaction. Int J Biol Macromol 2018;107(Pt A):790-795.

26. Figueiredo P, Lintinen K, Kiriazis A, Hynninen V, Liu Z, Bauleth-Ramos T, Rahikkala A, Correia A, Kohout T, Sarmento B and others. In vitro evaluation of biodegradable lignin-based nanoparticles for drug delivery and enhanced antiproliferation effect in cancer cells. Biomaterials 2017;121:97-108.

27. Tenzer S, Docter D, Kuharev J, Musyanovych A, Fetz V, Hecht R, Schlenk F, Fischer D, Kiouptsi K, Reinhardt C and others. Rapid formation of plasma protein corona critically affects nanoparticle pathophysiology. Nat Nanotechnol 2013;8(10):772-781.

28. Pino Pd, Pelaz B, Zhang Q, Maffre P, Nienhaus GU, Parak WJ. Protein corona formation around nanoparticles – from the past to the future. Mater Horiz 2014;1(3):301-313.

29. Monopoli MP, Walczyk D, Campbell A, Elia G, Lynch I, Bombelli FB, Dawson KA. Physical-chemical aspects of protein corona: relevance to in vitro and in vivo biological impacts of nanoparticles. J Am Chem Soc 2011;133(8):2525-2534.

30. Seabra AB, Bernardes JS, Favaro WJ, Paula AJ, Duran N. Cellulose nanocrystals as carriers in medicine and their toxicities: A review. Carbohydr Polym 2018;181:514-527.

31. Clift MJ, Foster EJ, Vanhecke D, Studer D, Wick P, Gehr P, Rothen-Rutishauser B, Weder C. Investigating the interaction of cellulose nanofibers derived from cotton with a sophisticated 3D human lung cell coculture. Biomacromolecules 2011;12(10):3666-3673.

32. Kai D, Ren W, Tian L, Chee PL, Liu Y, Ramakrishna S, Loh XJ. Engineering Poly(lactide)–Lignin Nanofibers with Antioxidant Activity for Biomedical Application. ACS Sustain Chem Eng 2016;4(10):5268-5276.

33. Jorfi M, Foster EJ. Recent advances in nanocellulose for biomedical applications. J Appl Polym Sci 2015;132(14):DOI:101002/app.41719.

34. Frohlich E. The role of surface charge in cellular uptake and cytotoxicity of medical nanoparticles. Int J Nanomedicine 2012;7:5577-5591.

35. Verma A, Stellacci F. Effect of surface properties on nanoparticle-cell interactions. Small 2010;6(1):12-21.

36. Imlimthan S, Otaru S, Keinanen O, Correia A, Lintinen K, Santos HA, Airaksinen AJ, Kostiainen MA, Sarparanta M. Radiolabeled Molecular Imaging Probes for the In Vivo Evaluation of Cellulose Nanocrystals for Biomedical Applications. Biomacromolecules 2019;20(2):674-683.

37. Sadeghifar H, Filpponen I, Clarke SP, Brougham DF, Argyropoulos DS. Production of cellulose nanocrystals using hydrobromic acid and click reactions on their surface. J Mater Sci 2011;46(22):7344-7355.

38. Lu P, Hsieh Y-L. Preparation and properties of cellulose nanocrystals: Rods, spheres, and network. Carbohydr Polym 2010;82(2):329-336.

39. Miyata K, Christie RJ, Kataoka K. Polymeric micelles for nano-scale drug delivery. React Funct Polym 2011;71(3):227-234.

40. Gaumet M, Vargas A, Gurny R, Delie F. Nanoparticles for drug delivery: the need for precision in reporting particle size parameters. Eur J Pharm Biopharm 2008;69(1):1-9.

41. Dufresne A. Nanocellulose: a new ageless bionanomaterial. Mater Today 2013;16(6):220-227.

42. Caixeiro S, Peruzzo M, Onelli OD, Vignolini S, Sapienza R. Disordered Cellulose-Based Nanostructures for Enhanced Light Scattering. ACS Appl Mater Interfaces 2017;9(9):7885-7890.

43. Duan X, Li Y. Physicochemical characteristics of nanoparticles affect circulation, biodistribution, cellular internalization, and trafficking. Small 2013;9(9-10):1521-32.

44. Arvizo RR, Miranda OR, Thompson MA, Pabelick CM, Bhattacharya R, Robertson JD, Rotello VM, Prakash YS, Mukherjee P. Effect of nanoparticle surface charge at the plasma membrane and beyond. Nano Lett 2010;10(7):2543-2548.

45. Alexis F, Pridgen E, Molnar LK, Farokhzad OC. Factors affecting the clearance and biodistribution of polymeric nanoparticles. Mol Pharm 2008;5(4):505-515.

46. Gustafson HH, Holt-Casper D, Grainger DW, Ghandehari H. Nanoparticle Uptake: The Phagocyte Problem. Nano Today 2015;10(4):487-510.

47. Tabish TA, Pranjol MZI, Jabeen F, Abdullah T, Latif A, Khalid A, Ali M, Hayat H, Winyard PG, Whatmore JL and others. Investigation into the toxic effects of graphene nanopores on lung cancer cells and biological tissues. Appl Mater Today 2018;12:389-401.

48. Evans ER, Bugga P, Asthana V, Drezek R. Metallic Nanoparticles for Cancer Immunotherapy. Mater Today (Kidlington) 2018;21(6):673-685.

49. Housman G, Byler S, Heerboth S, Lapinska K, Longacre M, Snyder N, Sarkar S. Drug resistance in cancer: an overview. Cancers (Basel) 2014;6(3):1769-1792.

50. Fulda S. Tumor resistance to apoptosis. Int J Cancer 2009;124(3):511-5.

51. Park MV, Lankveld DP, van Loveren H, de Jong WH. The status of in vitro toxicity studies in the risk assessment of nanomaterials. Nanomedicine (Lond) 2009;4(6):669-685.

52. Laaksonen T, Santos H, Vihola H, Salonen J, Riikonen J, Heikkila T, Peltonen L, Kumar N, Murzin DY, Lehto VP and others. Failure of MTT as a toxicity testing agent for mesoporous silicon microparticles. Chem Res Toxicol 2007;20(12):1913-1918.

53. Oh N, Park JH. Endocytosis and exocytosis of nanoparticles in mammalian cells. Int J Nanomedicine 2014;9 Suppl 1:51-63.

54. Yameen B, Choi WI, Vilos C, Swami A, Shi J, Farokhzad OC. Insight into nanoparticle cellular uptake and intracellular targeting. J Control Release 2014;190:485-499.

55. Behzadi S, Serpooshan V, Tao W, Hamaly MA, Alkawareek MY, Dreaden EC, Brown D, Alkilany AM, Farokhzad OC, Mahmoudi M. Cellular uptake of nanoparticles: journey inside the cell. Chem Soc Rev 2017;46(14):4218-4244.

56. Champion JA, Katare YK, Mitragotri S. Particle shape: a new design parameter for micro- and nanoscale drug delivery carriers. J Control Release 2007;121(1-2):3-9.

57. Jindal AB. The effect of particle shape on cellular interaction and drug delivery applications of micro- and nanoparticles. Int J Pharm 2017;532(1):450-465.

FIGURES, TABLES AND LEGENDS

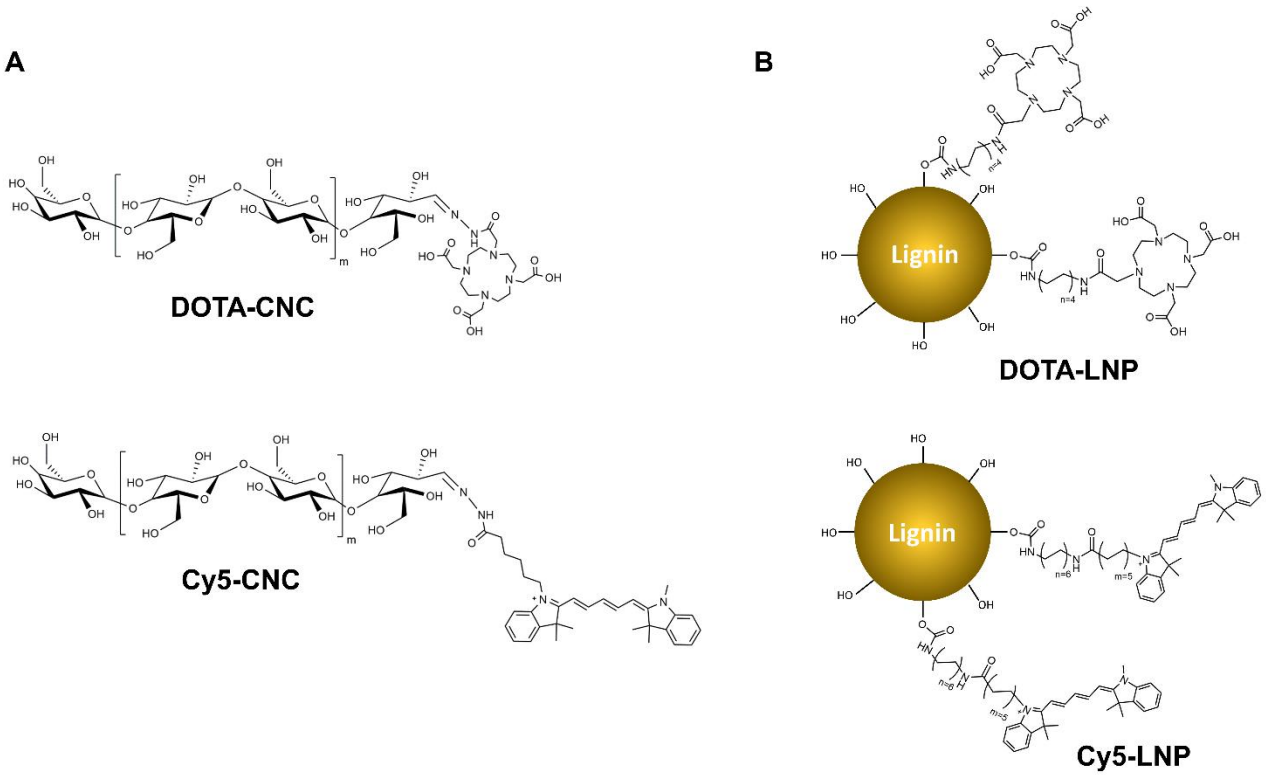

Scheme 1. The schematic representations of (**A**) DOTA- and Cy5-hydrazide modified CNC at the aldehyde terminal and (**B**) DOTA- and Cy5-amine modified lignin.

Table 1. Elemental analysis of unmodified and modified CNC and lignin nanoparticles (*n*=2 for each sample).

Samples	%C	%H	%N
Unmodified CNC	43.14–43.26	6.00–6.14	Not detected
DOTA-CNC	43.03–43.17	5.96–6.24	0.08–0.12
Cy5-CNC	43.48–43.52	6.09–6.17	0.09–0.11
Unmodified lignin	64.95–65.05	5.59–5.61	Not detected
DOTA-lignin	61.94–62.06	4.99–5.01	5.44–5.56
Cy5-lignin	64.49–64.51	5.38–5.62	1.39–1.61

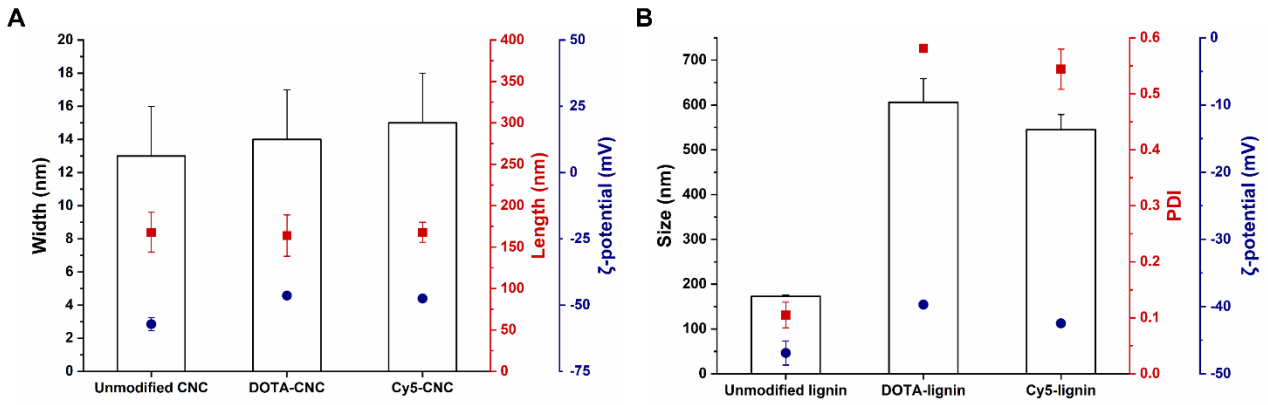

Figure 1. (**A**) Width (bar), length (square), and ζ-potential (dot) of CNC in aqueous solution (n=50), and (**B**) Size (bar), PDI (square) and ζ-potential (dot) of lignin NPs in aqueous solution. The results are presented as mean ± s.d. (n=3)

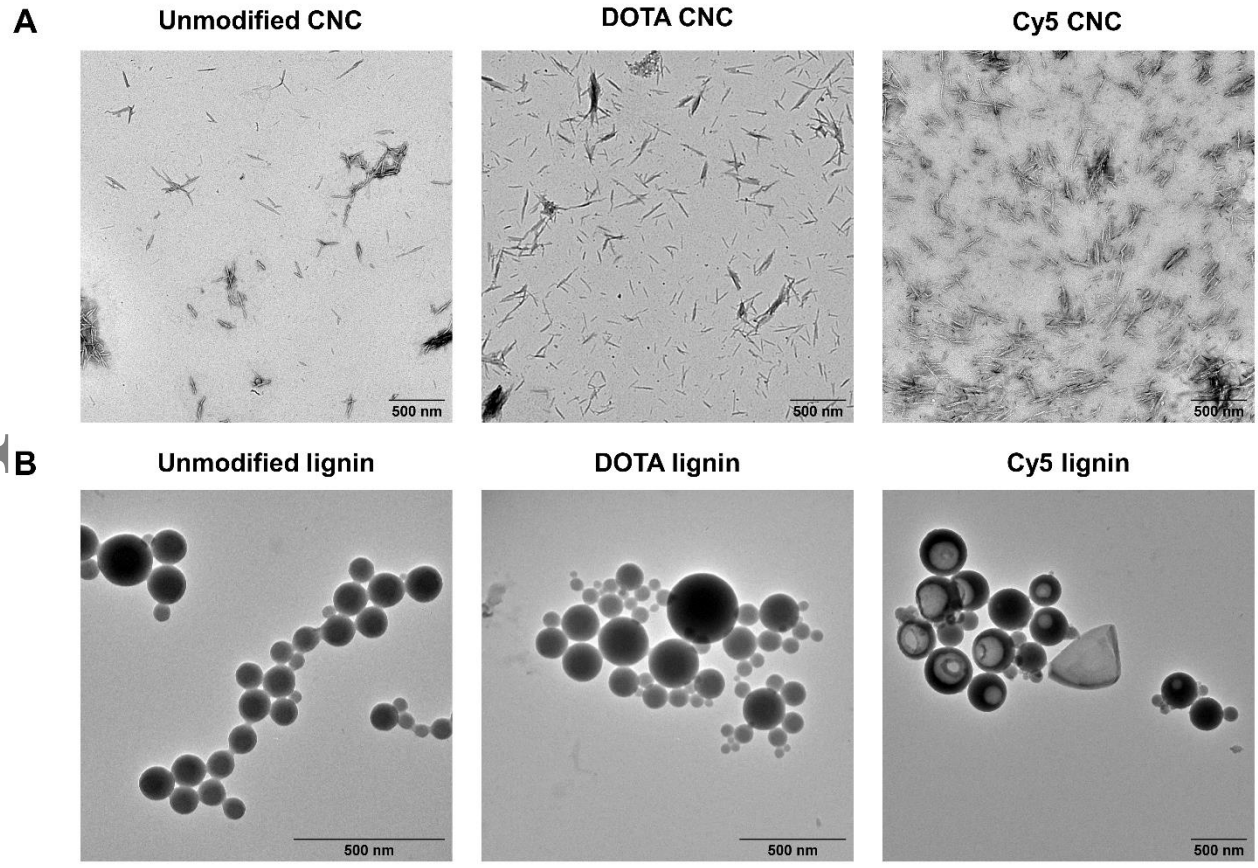

Figure 2. TEM images of CNC/lignin NPs in aqueous solution. (**A**) CNC NPs; unmodified CNC, DOTA-CNC and Cy5-CNC, and (**B**) Lignin NPs; unmodified lignin, DOTA-lignin, and Cy5-lignin.

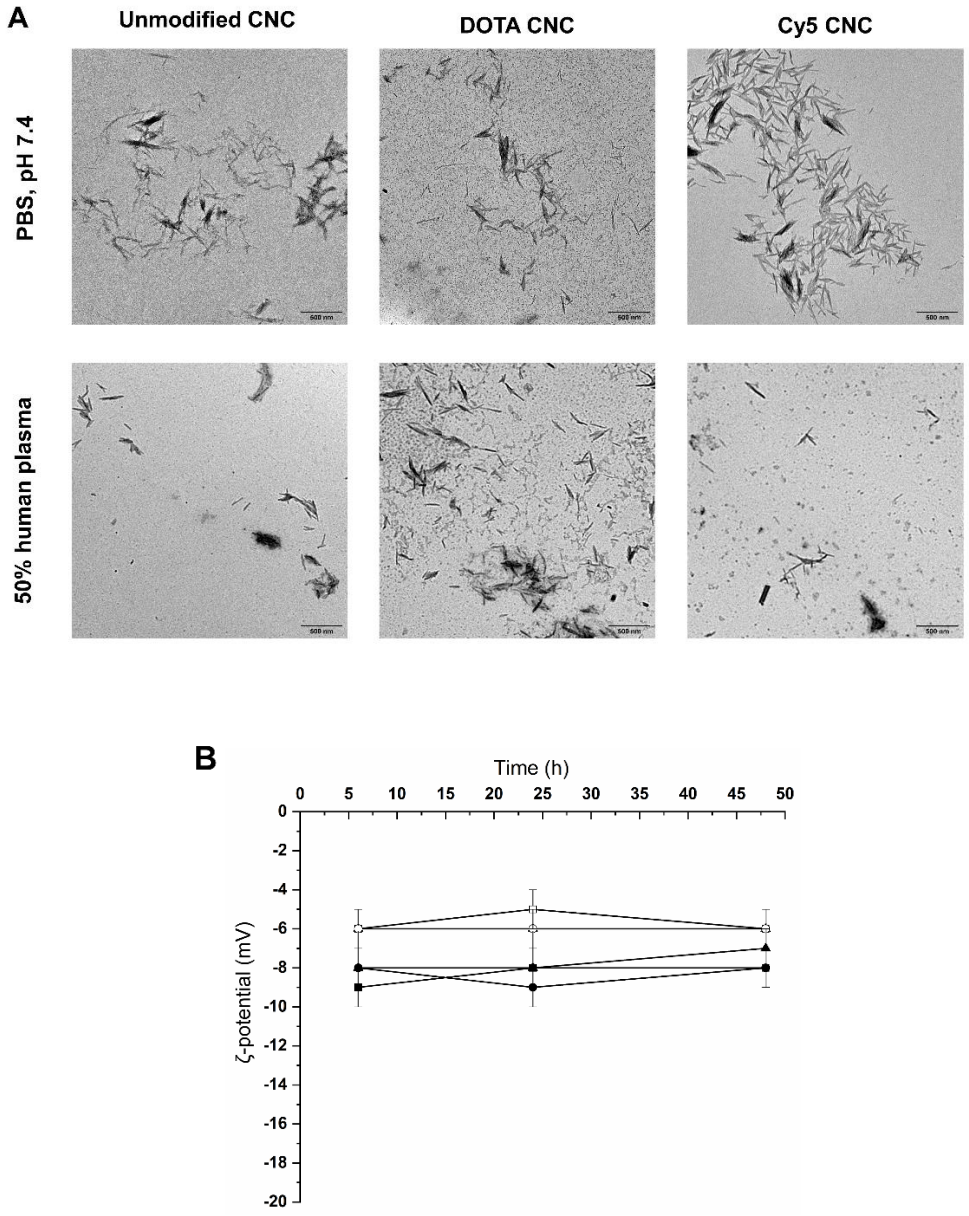

Figure 3. Stability of CNC NPs in PBS (pH 7.4) and 50% human plasma. (**A**) TEM images of CNC NPs after 48 h incubation (scale bar=500 nm), and (**B**) ζ-potential. The symbols denote unmodified CNC (square), DOTA-CNC (triangle), and Cy5-CNC (circle) NPs, and the filled symbols incubation in PBS (pH 7.4) and the closed symbols in 50% human plasma. Error bars represent mean ± s.d. (n=3).

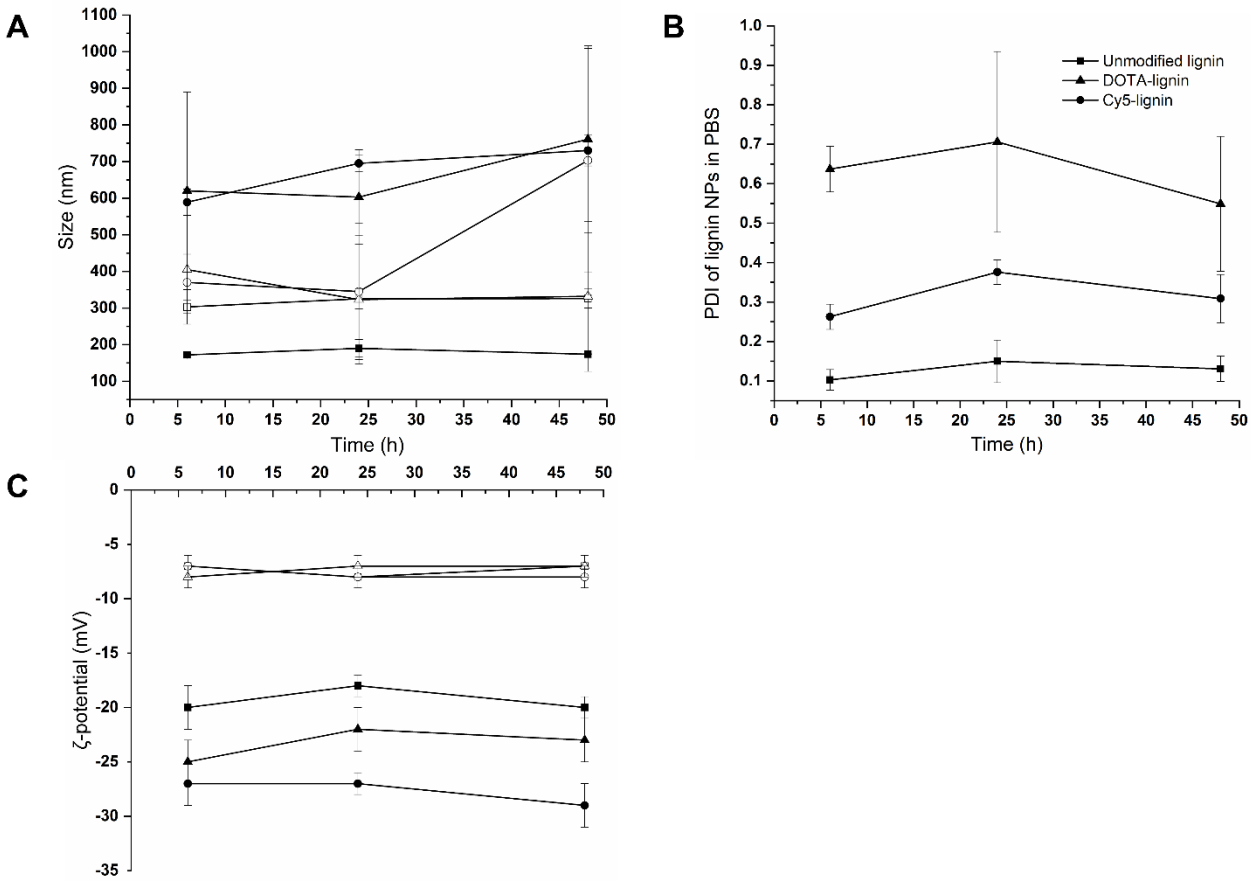

Figure 4. Stability of lignin NPs at 6, 24, and 48 h in PBS (pH 7.4, filled symbols) and 50% human plasma (open symbols). (**A**) Size, (**B**) PDI in PBS (pH 7.4), and (**C**) ζ-potential. The symbols denote unmodified lignin (square), DOTA-lignin (triangle), and Cy5-lignin (circle) NPs. Error bars represent mean ± s.d. (n=3).

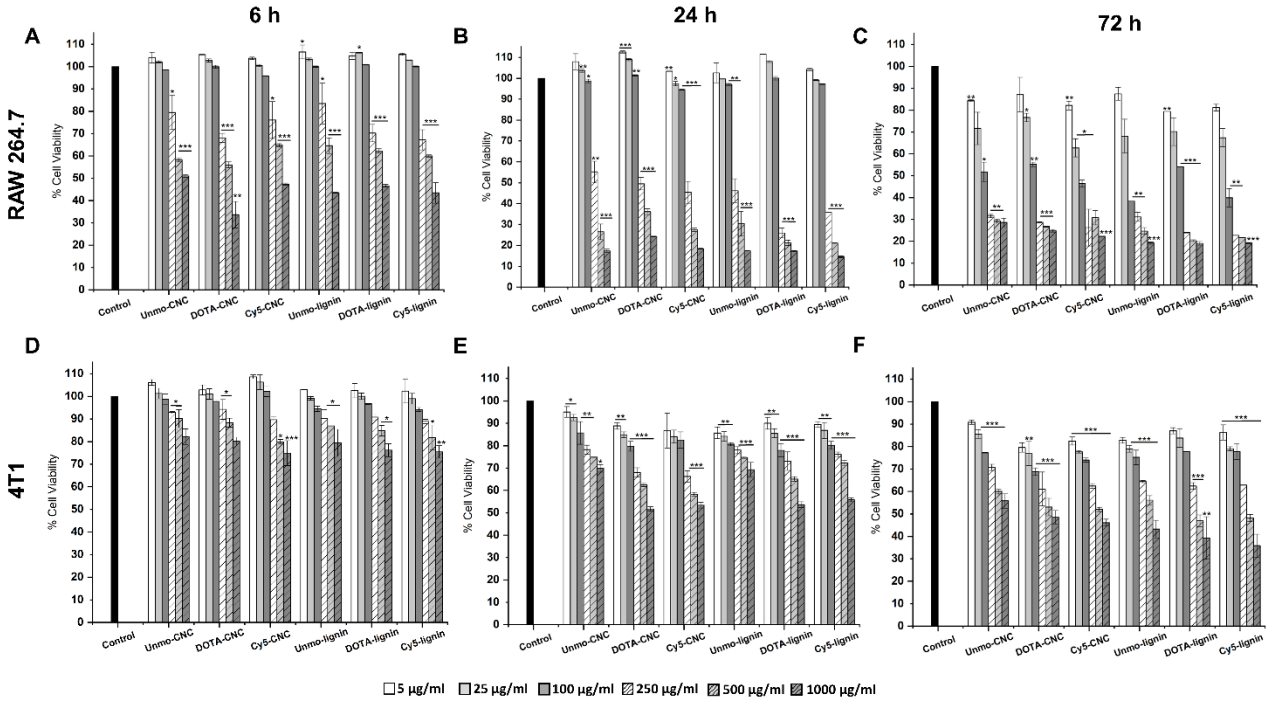

Figure 5. CellTiter-Glo® cell viability assay in RAW 264.7 macrophages (**A-C**) and 4T1 breast cancer cell lines (**D-F**) after incubation with unmodified CNC/lignin, DOTA-CNC/lignin, and Cy5-CNC/lignin NPs at low concentration (5, 25, and 100 µg/ml) and high concentration (250, 500, and 1000 µg/ml) ranges for 6, 24, and 72 h. The control is treated with medium only and the viability set to 100%. Error bars represent the mean ± s.d. (n=3). The statistical hypothesis was evaluated by Student's *t*-test where the significant probabilities were set at $^{*}p < 0.05$, $^{**}p < 0.01$ and $^{***}p < 0.001$.

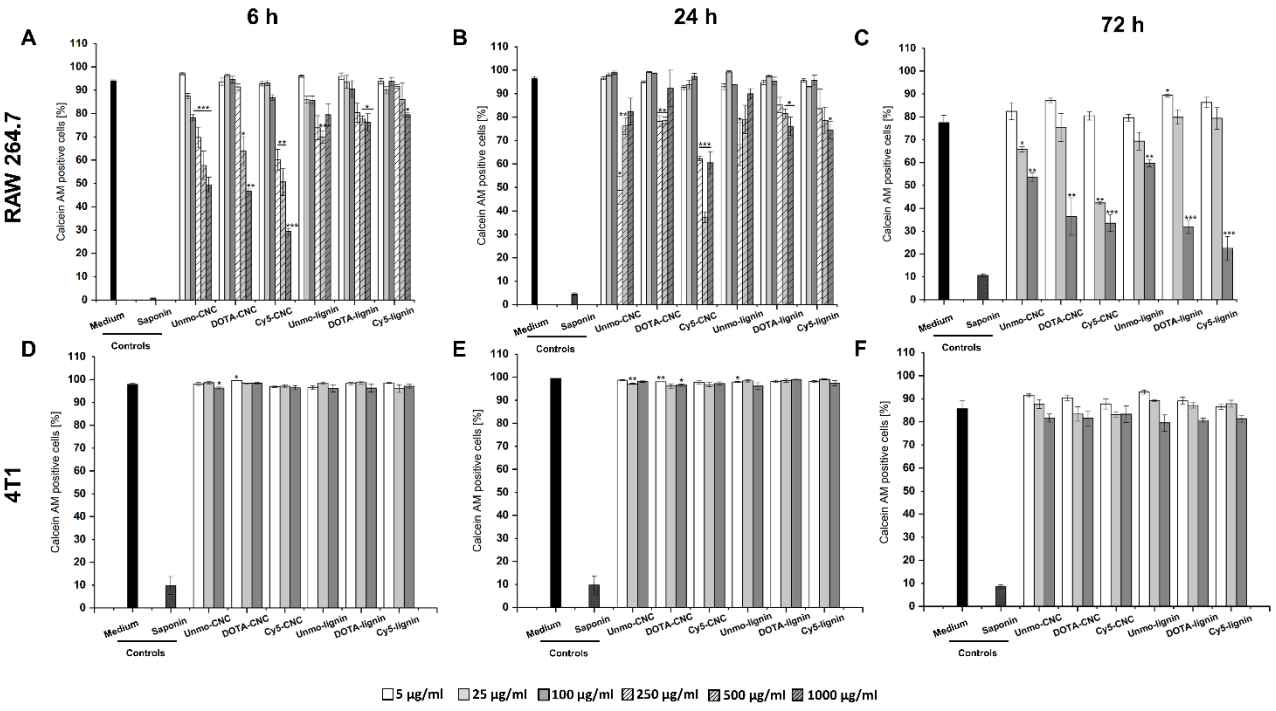

Figure 6. LIVE/DEAD® cell viability assay in RAW 264.7 macrophages (**A-C**) and 4T1 breast cancer cell lines (**D-F**) after incubation with unmodified CNC/lignin, DOTA-CNC/lignin, and Cy5-CNC/lignin NPs at low concentration (5, 25, and 100 µg/ml) and high concentration (250, 500, and 1000 µg/ml) ranges for 6, 24, and 72 h. Culture medium and 0.1% (w/w) saponin were used as negative and positive controls for cytotoxicity, respectively. Error bars represent the mean ± s.d. (n=3). The statistical hypothesis was evaluated by Student's *t*-test where the significant probabilities were set at $^{*}p < 0.05$, $^{**}p < 0.01$ and $^{***}p < 0.001$.

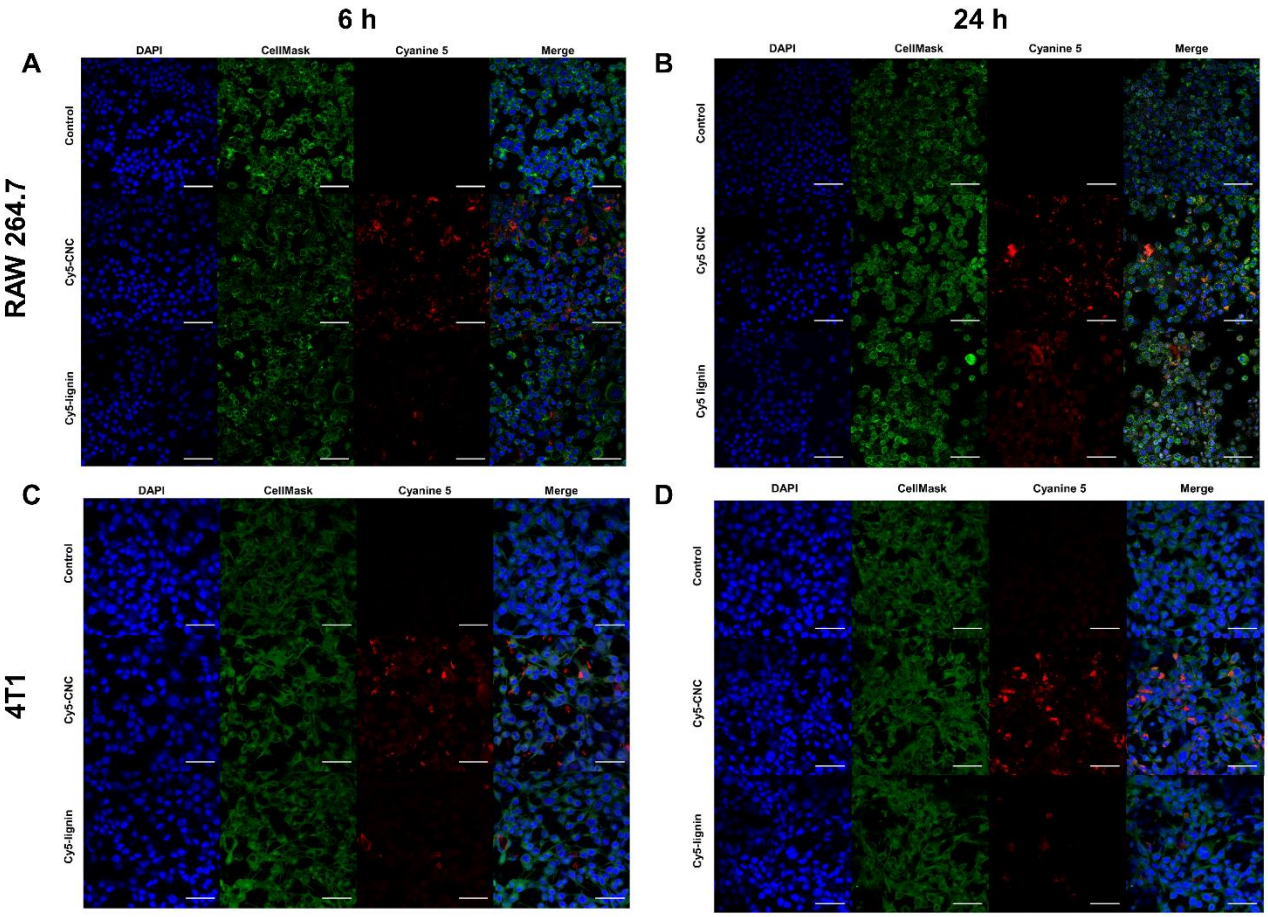

Figure 7. Cell–NP interactions visualized by confocal microscopy of RAW 264.7 macrophages (**A and B**) and 4T1 breast cancer cells (**C and D**) after incubation with Cy5-CNC and Cy5-lignin NPs at 100 µg/ml for 6 and 24 h. DAPI (blue), CellMask™ Green (green), and Cy5 (red) indicate nucleus, plasma membrane and NPs, respectively. The images were taken at 63× magnification (scale bar=50 µm).